PHYSICAL REVIEW B VOLUME 50, NUMBER 3 15 JULY 1994-I

Photogenerated carrier dynamics under the influence of electric fields in III-V semiconductors

Y. Rosenwaks, B. R. Thacker, R. K. Ahrenkiel, and A. J. Nozik
National Renewable Energy Laboratory, Golden, Colorado 80401

I. Yavneh
Department of Computer Sciences, Technion, Haifa 32000, Israel

(Received 7 March 1994)

We present a rigorous analysis of the effects of electric fields on time-resolved photoluminescence spectra in semiconductors. It is based on the solution of the semiconductor transport equations using the drift-diffusion approxmation. The results show that the effect of the field alone on the photoluminescence decay can be distinguished from that of charge separation and field-enhanced surface recombination. The analysis is applied to two different sets of experiments. In the first, we use femtosecond luminescence upconversion to observe the ultrafast charge separation in the space-charge region, and screening of the electric field under high-injection conditions. The second group of experiments was conducted on heterostructures of $GaAs/Ga_xIn_{1-x}P$ under externally applied bias using time-correlated single-photon counting detection in the picosecond time domain. The use of the method for extracting charge-transfer velocities across semiconductor interfaces is discussed.

I. INTRODUCTION

Recently there has been considerable interest in studying photogenerated carrier dynamics in semiconductors under the influence of electric fields. This is a process of critical importance in recombination kinetics and electron transfer processes at semiconductor interfaces. Various issues such as electroneutrality,[1] screening of surface space-charge fields,[2] carrier sweep-out in quantum structures,[3] and carrier injection across semiconductor-liquid interfaces[4] are of interest. The last is vital for understanding the fundamental processes of charge transfer at semiconductor-liquid interfaces, and for determining the role of the electric field in this process. Furthermore, it is still necessary to clarify the role of hot carriers in this process,[5–7] and how are they affected by the field.

Photogenerated carrier dynamics can be studied by various optical methods.[8] In recent years time-resolved photoluminescence (TRPL) has become one of the most widely used techniques to measure carrier dynamics in the picosecond and nanosecond time scales.[9] Fundamental parameters such as minority-carrier lifetime,[10] surface recombination velocity (SRV),[11] and carrier cooling dynamics,[12] are determined by TRPL. However, to date the analysis and interpretation of TRPL data obtained in the presence of electric fields has been lacking. This is because the inclusion of electric-field terms in the continuity equations that describe excess carrier dynamics in semiconductors greatly complicates their solution.

Experiments designed to study carrier dynamics are frequently conducted under conditions which tend to minimize the effects of electric fields.[13] This is done in order to simplify the carrier dynamics analysis; when the electric field cannot be neglected, the electron and hole concentrations [needed for calculating the photoluminescence (PL) intensity] have to be calculated from the two continuity equations coupled through Poisson's equation (see below). This is a system of stiffly coupled nonlinear partial differential equations which have no analytical solutions; moreover, the numerical solutions require appreciable computer time.

The two most widely used experimental conditions to overcome the above difficulty are to conduct the TRPL measurements under very high or very low carrier-injection levels. In the first case the field in the space-charge region (SCR) is screened by the high density of photogenerated carriers, and the two continuity equations can be replaced by the well-known ambipolar continuity equation.[14] While this approach has shown fairly good agreement with experimental data,[15,16] it has several drawbacks. First, the electric field in the SCR is not totally screened even under very-high-injection conditions, and the screening decreases with time as the excess carrier concentration changes. Second, for medium- or high-doped samples the experiments have to be carried out under very high carrier injection levels; this can introduce further complications in the analysis related to carrier degeneracy, band-filling effects, and Auger recombination. Third, the high laser photon fluxes used in such experiments can cause radiation damage and heating of the samples.

Under low-injection conditions the TRPL data are typically analyzed by treating only the minority-carrier transport and solving only one continuity equation in the field free region.[17,18] This is usually justified by assuming that (1) luminescence emitted from the SCR can be neglected; (2) the electric field in the SCR is constant with time; (3) the electric field created by the spatial separation of the excess carriers can be neglected; and (4) any field effects can be treated by assigning an effective recombination velocity S_{eff} to the minority carriers at the SCR edge.

However, TRPL experiments are frequently conducted

0163-1829/94/50(3)/1746(9)/$06.00 ©1994 The American Physical Society

under carrier injection levels which do not satisfy the above conditions, especially when the semiconductor doping level is moderate or low, and/or sub-50-ps time resolution is desired.[19] More important, in certain situations it is desirable to study the effect of the electric field on various semiconductor phenomena; hence the electric-field terms must be included in the analysis.

In this study we conduct a self-consistent calculation of the effect of electric fields on TRPL emitted from a semiconductor following excitation by a short laser pulse. Applying the analysis to two different sets of experiments, we demonstrate very good agreement with the model. Our numerical model is described in Sec. II. Section III describes calculations of the TRPL spectra in the presence of electric fields under high-, intermediate-, and low-injection levels. A comparison with two sets of experimental results is presented in Sec. IV, and the manuscript is summarized in Sec. V.

II. MODEL

The sample and measurement setup are schematically illustrated in Fig. 1(a). The TRPL is collected using the front geometry mode, and measured as a function of an external applied bias, V_{so}, and under different injection levels. Figure 1(b) shows a schematic picture of the charge-density distribution in the sample right after the laser pulse at $t>0$. The charge density includes the ionized acceptors (for p-type samples) in the SCR which compensates the surface charge N_s and the photogenerated electron-hole pairs. At $t>0$ electron-hole pairs are generated by the laser pulse, and their initial distribution (before any diffusion or drift takes place) is determined by the absorption depth $1/\alpha$. Our model calculates the PL intensity which is determined by the overall charge distribution as a function of time following the laser excitation.

Figure 2 presents the semiconductor band diagram

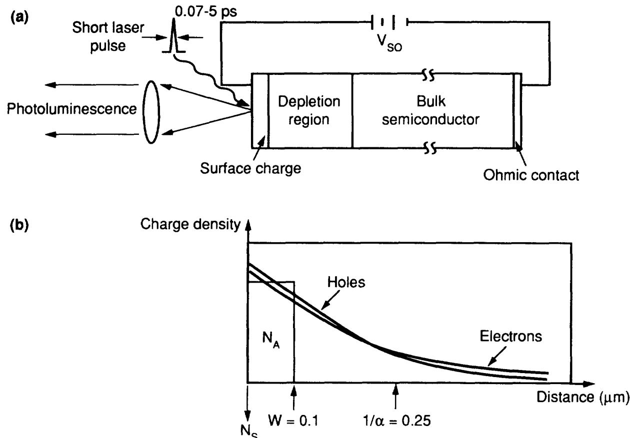

FIG. 1. (a) Sketch of the photoluminescence measurement setup. (b) The charge-density distribution as a function of distance from the crystal surface right after the laser excitation, at $t>0$. N_s is the surface state density, N_A the ionized acceptor density, W the width of the space charge region, and α the absorption coefficient.

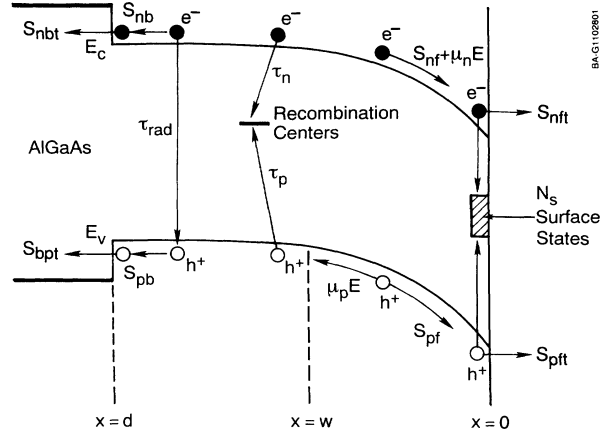

FIG. 2. Energy-band diagram of a typical heterostructure used in our analysis.

used in our calculations. It is a typical heterostructure, widely used as a diagnostic prototype for TRPL measurements and analysis, consisting of an active layer which absorbs the light, sandwiched on one side by a larger band-gap semiconductor that acts as a confinement layer for minority carriers, and on the other side by a second phase (air, solution, or another semiconductor confinement layer). We start by calculating the electric field in the active layer prior to optical excitation, $E(x,t<0)$; this is done using a one-dimensional Poisson equation solver with appropriate boundary conditions determined by the geometrical configuration.

Following the excitation, the bulk transport of electrons and holes is modeled using the standard drift-diffusion approximation for the carrier distributions. This is a simple formulation of the Boltzmann transport equation derived in the relaxation-time approximation;[20] therefore the carrier distributions are treated as instantaneously thermalized, and are described by average transport parameters. Hence the basic equations are the continuity and Poisson equations:

$$\frac{\partial n(x,t)}{\partial t}=g(x,t)+D_n\frac{\partial^2 n(x,t)}{\partial x^2}+\mu_n\frac{\partial}{\partial x}[E(x,t)n(x,t)]-R_n\ , \tag{1}$$

$$\frac{\partial p(x,t)}{\partial t}=g(x,t)+D_p\frac{\partial^2 p(x,t)}{\partial x^2}-\mu_p\frac{\partial}{\partial x}[E(x,t)p(x,t)]-R_p\ , \tag{2}$$

$$\frac{\partial E(x,t)}{\partial x}=\frac{q}{\epsilon}[p(x,t)-n(x,t)+N_d(x)-N_a(x)]\ , \tag{3}$$

where $n(x,t)$ and $p(x,t)$ are the bulk densities of electrons and holes, D_n and D_p are the diffusion coefficients for electrons and holes, μ_n and μ_p are their mobilities, q is the electron charge, ϵ is the bulk static dielectric constant, and N_d and N_a are the densities of donor and acceptor ions, respectively. Since the SCR fields can reach values in the range of tens or hundreds kV/cm, satura-

tion of the drift velocity can occur; therefore the free-carrier drift velocities $v_d(x,t)$ $[v_d=\mu E(x,t)]$ were limited to 2×10^7 cm/s (saturated value) by adjusting μ_n and μ_p as the field increased to the saturated velocity region. $g(x,t)$ is the optical generation term, which is calculated from the laser intensity profile $I(t)$ via

$$g(x,t)=I(t)\alpha(1-R)e^{-\alpha x}\ , \tag{4}$$

where R is the sample reflectivity, and α is the absorption coefficient. R_n and R_p represent the bulk recombination rates for electrons and holes given, for example, for electrons as

$$R_n=B[n(x,t)+N_d(x)][p(x,t)+N_a(x)]+\frac{n(x,t)}{\tau_n}\ , \tag{5}$$

where B is the radiative recombination rate constant, and τ_n is the Shockley-Read-Hall (SRH) nonradiative lifetime for electrons. Auger recombination was not included in the calculations because it can be neglected at the moderate doping and excitation levels used in this study.[21]

The surface dynamics is coupled to the bulk dynamics by equating the carrier flux toward each surface to the surface current. The electron flux J_n at $x=0$ is given by

$$\begin{aligned} J_n&=-qD_n\frac{\partial n}{\partial x}\bigg|_{x=0}-q\mu_n n(x=0)E_s \\ &=-qn(x=0)(S_{nf}+S_{nft})\ , \end{aligned} \tag{6}$$

where the term on the right-hand side is the electron surface current at $x=0$. Rearranging terms and repeating the procedure for the interface at $x=d$ and including holes results in four boundary conditions:

$$\begin{aligned} \frac{\partial n}{\partial x}\bigg|_{x=0}&=\frac{(S_{nf}+S_{nft}-\mu_n E_s)}{D_n}n\quad (x=0,t)\ , \\ \frac{\partial p}{\partial x}\bigg|_{x=0}&=\frac{(S_{pf}+S_{pft}+\mu_p E_s)}{D_p}p\quad (x=0,t)\ , \end{aligned} \tag{7}$$

$$\begin{aligned} \frac{\partial n}{\partial x}\bigg|_{x=d}&=-\frac{(S_{nb}+S_{nbt}+\mu_n E_d)}{D_n}n\quad (x=d,t)\ , \\ \frac{\partial p}{\partial x}\bigg|_{x=d}&=-\frac{(S_{pb}+S_{pbt}-\mu_p E_d)}{D_p}p\quad (x=d,t) \end{aligned} \tag{8}$$

where S_{nf} and S_{pf} are the front surface (at $x=0$) recombination velocities (SRV) for electrons and holes, respectively, S_{nb} and S_{pb} are the SRV's at the back interface ($x=d$), and E_s and E_d are the fields at $x=0$ and d, respectively. A free carrier reaching an interface can either recombine or be transmitted across it (either by tunneling mechanisms or by thermionic emission); this is represented here by a carrier transfer velocity, S_{nft} and S_{pft} for electrons and holes, respectively, at $x=0$, and by S_{nbt} and S_{pbt} at $x=d$.

The electric field at the interface changes if a free carrier is trapped at an interface state before it recombines with the other carrier type, or is transferred across the interface. Hence the electric field at any interface at times $t>0$ is calculated (for example at $x=0$ and $t=t_1$) using Gauss law as

$$E_s(t=t_1)=\frac{q}{\epsilon}[p_s(t_1)-n_s(t_1)\pm N_s]\ , \tag{9}$$

where N_s is the surface fixed charge, and $p_s(t_1)$ and $n_s(t_1)$ are the concentrations per unit area of holes and electrons trapped at the surface after time t_1, calculated for example for electrons as

$$n_s(t_1)=\int_0^{t_1}n(x=0,t)S_{nf}(t)dt\ . \tag{10}$$

The SRV's and τ's contain all mechanisms describing the interaction between the free carriers and a recombination center, and no attempt is made here either to calculate their values from microscopic properties,[11] or to include their dependence on the SRH parameters.

The continuity and Poisson equations [Eqs. (1), (2), and (3)] are solved using a finite difference semi-implicit algorithm on a Cray-2 supercomputer, to give $n(x,t)$ and $p(x,t)$. The TRPL $I(t)$ is then calculated as

$$I(t)=\int_0^d[n(x,t)p(x,t)]e^{-\alpha_L x}dx\ , \tag{11}$$

where α_L is the absorption coefficient at the PL wavelength, and d is the active layer thickness. In order to maintain numerical stability the time steps were limited to around 10 fs, and the space steps are restrained to about 20 Å to avoid degrading the solution accuracy.

III. TRPL CALCULATED IN THE PRESENCE OF ELECTRIC FIELDS

A. High-injection level, $I_0=10$

Figure 3 shows normalized TRPL decay curves calculated for three different initial dark (at $t<0$ and at $x=0$) band-bending (V_{so}) values of 0.0, 0.3, and 0.6 V. The injection level (I_0), defined here as the ratio between the initial (at $t=0$) photogenerated excess carrier concentration and the semiconductor majority-carrier concentration, was 10. The calculations were carried out for a GaAs/Al_xGa_{1-x}As heterostructure (such as the one shown in Fig. 2) using the following parameters: $d=0.5$

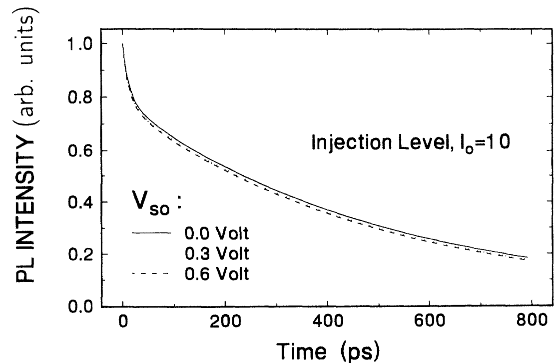

FIG. 3. Normalized TRPL spectra under high injection level ($I_0=10$) calculated for three different initial band-bending values V_{so}.

μm, $\alpha = 4\times10^4$ cm^{-1}, $\alpha_L = 1\times10^3$ cm^{-1}, $\mu_n = 3800$ cm^{2}V^{-1}s^{-1}, $\mu_p = 200$ cm^{2}V^{-1}s^{-1}, $B = 2\times10^{-10}$ cm^{3}s^{-1}, $\tau_n = \tau_p = 1$ ns, $S_{nf} = S_{pf} = 1000$ cm/s, and $S_{nb} = S_{pb}$ (the SRV's at $x = d$) = 100 cm/s. The GaAs layer was p type, with a doping density of 5×10^{16} cm^{-3}; the band bending at the back interface (at $x = d$) was assumed to be zero by appropriate adjustment of the $Al_xGa_{-1x}As$ doping density. A $\delta(t)$ laser pulse was used.

For $I_0 = 10$ the effect of V_{so} on the PL lifetime τ_{pl} is very small. This is because the electric field in the SCR is instantaneously screened by the separation of photogenerated charge carriers. This is demonstrated in Fig. 4, which shows the electric field [Fig. 4(a)] and the electron and hole distributions [Figs. 4(b) and 4(c)] at $t = 0$, and at times of 0.1, 1, and 10 ps following the excitation. Figures 4(b) and 4(c) show that at $t = 0.1$ ps the electron concentration at the surface greatly increases, while the hole distribution is peaked at a distance of around 150 Å from the surface. At this point the electric field due to the electron-hole spatial separation becomes comparable in magnitude to the initial field (but of opposite sign), and hence the net field is screened throughout the SCR as shown by the curve for $t = 0.1$ ps in Fig. 4(a). Thus, when the field in the SCR becomes very small the carriers will start to diffuse (rather than drifting in opposite directions), and their distributions will become flatter with time, as shown in Figs. 4(b) and 4(c). Since this transition from field- to diffusion-controlled transport is so fast (starting after about 0.1 ps), it is hardly observed in the PL decay in Fig. 3.

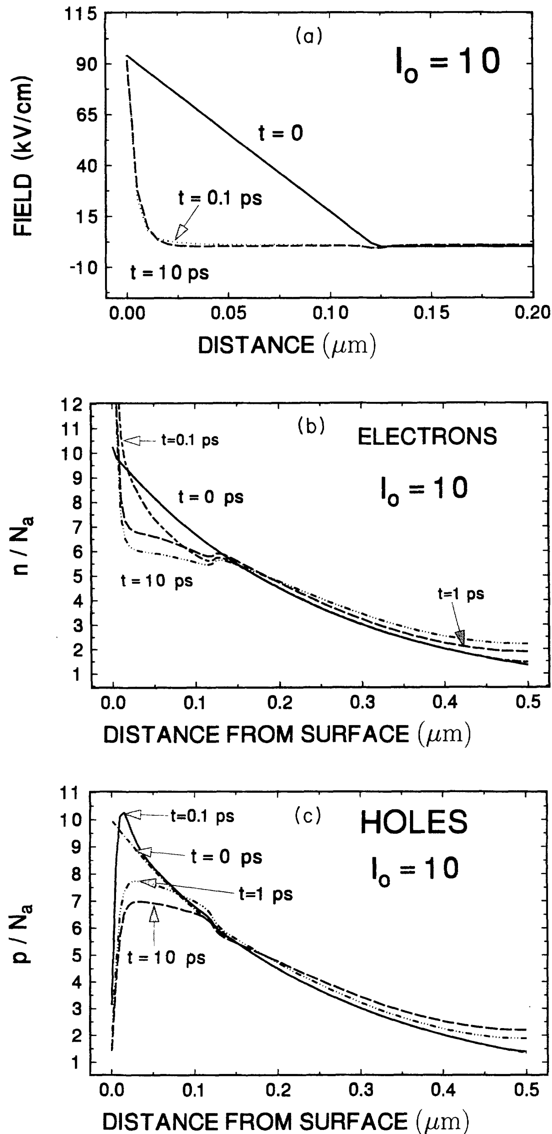

FIG. 4. (a) Electric-field profiles calculated before the laser pulse ($t = 0$), and at $t = 0.1$ (dotted line) and 10 ps after the excitation. The initial dark band bending V_{so} was 0.6 V. (b) Excess electrons distributions (normalized to the majority-carrier concentration N_a) at four different times after the excitation: $t = 0$, 0.1, 1, and 10 ps. (c) Excess hole distributions at the same times as in (b).

As can be seen from Fig. 4(a) the electric field near $x = 0$ is hardly affected; this is due to the fixed surface charge N_s. The surface electric field will decrease only when the concentration of electrons trapped at the surface, n_s, is large enough to affect N_s [see Eq. (9)]. This process, known as surface-state charging, is usually relatively slow. This is because when an electron is trapped at the surface it will recombine with a hole or be transferred to the adjacent medium; only when $S_{nf} \gg$ both S_{nft} and S_{pf} will the surface charge quickly. However, this will occur on the picosecond time scale only when S_{nf} is above 1×10^6 cm/s.

B. Intermediate-injection level, $I_0 = 1$

Figure 5 shows normalized TRPL curves calculated for an initial injection level I_0 of 1; all the other parameters were the same as in Fig. 3. For this case, the PL decay profile is clearly affected by the external field, and the transition from drift- to diffusion-controlled transport is easily observed. The reason for this is that now there are not enough excess carriers to screen the field immediately, and a relatively large field (>2 kV/cm) exists

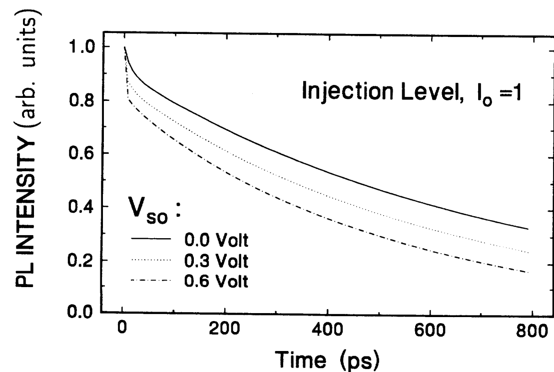

FIG. 5. Normalized TRPL spectra under an intermediate injection level ($I_0 = 1$) calculated for three different initial band-bending values V_{so}.

throughout the SCR during the first ps following the excitation; this is demonstrated in Fig. 6(a), which shows the electric-field distributions at four different times following the laser pulse.

The value of the electric field at which carrier diffusion dominates can be estimated from the continuity equations [Eqs. (1) or (2)] by comparing the magnitudes of the diffusion and drift terms (the second and third terms on the right-hand side, respectively) of either of the equations. If we assume an exponential carrier distribution of the form given by Eq. (4), (which is the carrier distribution right after the laser pulse), and calculate the ratio between the diffusion and drift terms, we find that diffusion will be dominant if $kT/\alpha > E$. Using an α value of 4×10^4 cm^{-1} this will occur when $E<1$ kV/cm. Figure 6(a) shows that this condition is satisfied only at times greater than 1 ps; this is when the PL decay rate greatly decreases, as can be observed from Fig. 5.

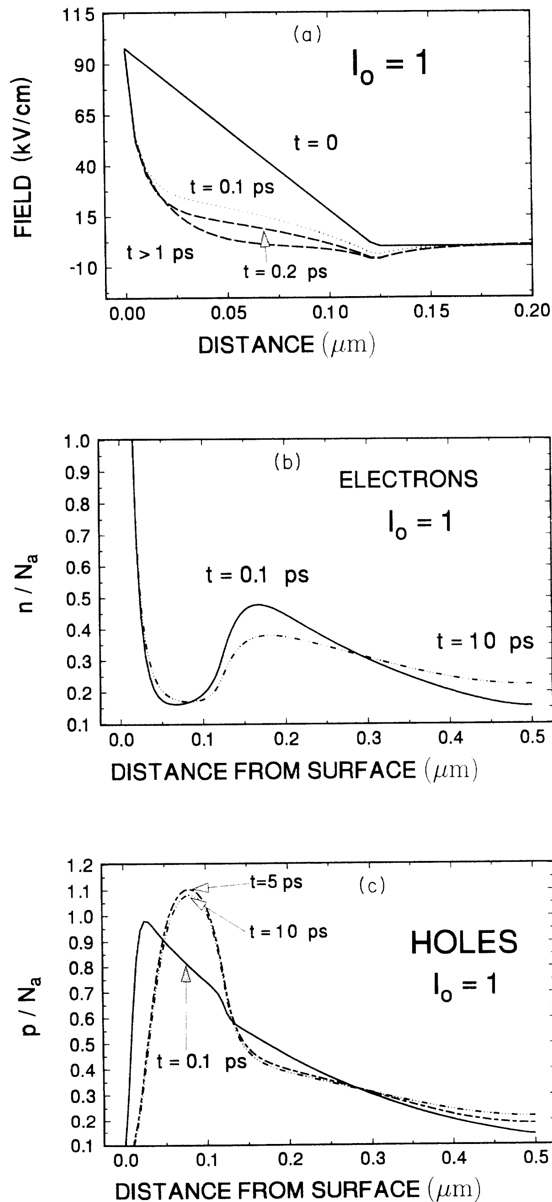

FIG. 6. (a) Electric-field profiles calculated at four different times relative to the laser pulse (at $t=0$). The initial dark band bending V_{so} was 0.6 V. (b) Excess electrons distributions (normalized to the majority-carrier concentration N_a) at two different times after the excitation: $t=0.1$ and 10 ps. (c) Excess hole distributions at times of 0.1, 5, and 10 ps following the excitation.

Figure 6(b) shows electron distributions at times of 0.1 and 10 ps, and Fig. 6(c) the hole distributions at times of 0.1, 5, and 10 ps following the excitation. It can be seen that the holes are pushed toward the back edge of the SCR in a few ps, and only then does the peak of their distribution decrease; this is evidence of diffusion. Holes and electrons outside the SCR ($x>0.15$ μm) start to diffuse right away because the field in this region is $\ll 1$ Kv/cm, as shown in Fig. 6(a). Following the initial charge separation and the resulting fast PL drop, the TRPL becomes diffusion controlled, and the decay rate is very similar to that in Fig. 3 (the high-injection-level case).

Comparison of Figs. 6(b) and 6(c) to Figs. 4(b) and 4(c) further illustrates the difference between the high- and intermediate-injection levels. In Fig. 4 the electron and hole distributions in the SCR ($x<0.1$ μ) become flatter after 0.1 ps because of diffusion. In Fig. 6, on the other hand, the electron distribution in the SCR hardly changes in the first 10 ps, while the holes start to diffuse only after they accumulate at the edge of the SCR region after about 5 ps.

C. Low-injection level, $I_0=0.1$

At the lowest injection level ($I_0=0.1$, Fig. 7) the shape of the TRPL curves is quite different. This is caused by the fact that the SCR field is not screened in this case. This is shown in Fig. 8, which shows the electric field calculated at this injection level at $t=0$ and at 10 ps following the laser pulse. The SCR field causes a faster PL decay compared with the higher injection levels in the same time period; this is because the minority carriers are

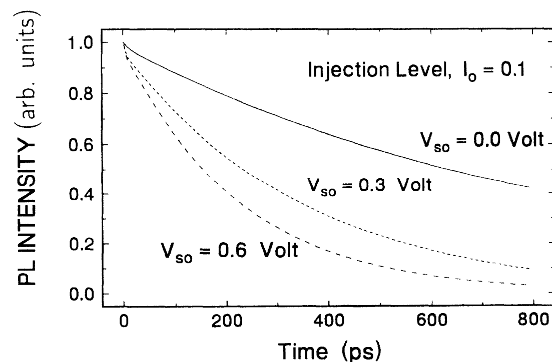

FIG. 7. Normalized TRPL spectra under a low injection level ($I_0=0.1$) calculated for three different initial band-bending values.

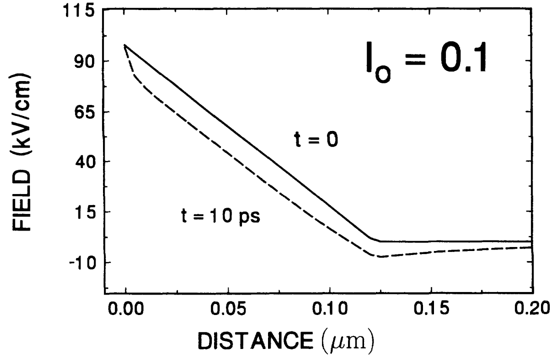

FIG. 8. Electric-field profiles calculated at an injection level of $I_0=0.1$. The initial dark band bending V_{so} was 0.6 V.

swept toward the surface with an effective SRV (S_{eff}), which is larger than S_{nf}; larger SRV's increase the PL decay rate. S_{eff} is defined as the interface recombination velocity at the edge of the SCR region (at $x=W$); it can be viewed as the velocity with which the carrier crosses the boundary between the bulk and the SCR.

To summarize the effect of band bending on the TRPL decay profiles at different injection levels, it would be instructive to examine the calculations presented in Fig. 9. The figure shows the band bending at the surface [$V_s(t)$] calculated at the three different injection levels ($I_0=10$, 1, and 0.1) for a V_{so} of 0.6 V; this was done by integrating the total electric field throughout the active layer as a function of time. For $I_0=10$, V_s is reduced to below 0.1 V in about 0.1 ps [in agreement with Fig. 4(a)]; thus the PL decay is diffusion controlled at all times greater than 0.1 ps. When $I_0=1$, V_s is reduced to about 0.12 V within 1 ps; during this time period the PL decays very quickly due to the charge separation, and then slows similarly in the high injection case. At the low injection level ($I_0=0.1$) the surface band bending is reduced only to about 0.4 V; thus the luminescence decay is controlled by surface recombination at all times.

IV. COMPARISON WITH EXPERIMENTAL RESULTS

We compare our calculations with two different sets of experiments. The first is aimed at observing the ultrafast charge separation in the SCR on the subpicosecond time scale and the screening of the electric field under high-injection conditions; these experiments were conducted under open-circuit conditions. The purpose of the second group of experiments is to observe the effect of an accurately controlled external applied bias on the PL decay under closed-circuit conditions on the picosecond time scale.

A. Luminescence up-conversion—femtosecond time resolution

The sample used was *p*-InP (Zn doped, 1.5×10^{17} cm^{-3}) single crystals with (100) surface orientation (from Nippon Mining). They were etched for 30 in 2% Br_2/MeOH and then measured in air. Time-resolved PL (TRPL) spectra were obtained by the technique of sum frequency generation.[19] Photoexcitation was with a Ti:sapphire laser that provided 80-fs pulses at a wavelength of 780 nm, and a 82-Mhz repetition rate. The laser spot size was $\approx 20\ \mu$ in diameter, and the temporal resolution of the system was 100 fs.

Figure 10 shows the TRPL spectra of the InP sample measured in air at two different laser intensities corresponding to excess carrier concentrations of 5×10^{18} and 2×10^{17} cm^{-3}. The solid lines were calculated using the following known parameters: $\alpha=2.5\times10^4$ cm^{-1}, $\alpha_L=1\times10^3$ cm^{-1}; $\mu_n=1900$ cm^2 V^{-1} s^{-1}, $\mu_p=100$ cm^2 V^{-1} s^{-1}, $B=2\times10^{-10}$ cm^3 s^{-1}, and $\tau_n=\tau_p=0.5$ ns; selection of the values of the above fixed parameters were based on a recent study of InP.[21] A $\delta(t)$ laser pulse was assumed, and V_{so} (the initial surface band bending in the dark) was 0.5 V, which is typical of the air/*p*-InP interface. The initial injection level I_0 was 30 and 1 for the upper and lower curves, respectively; this was calculated from the measured laser spot size and incident laser power. The values of the two adjustable parameters S_{nf}

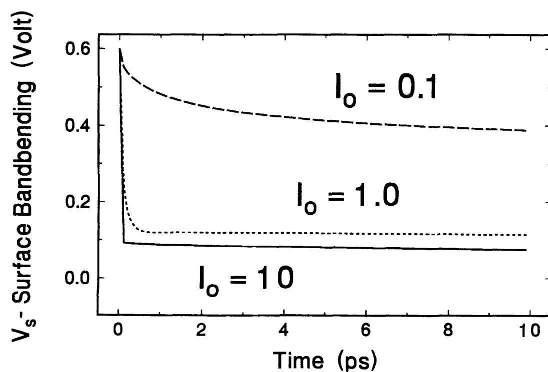

FIG. 9. Surface band bending as a function of time following the excitation calculated for the three different injection levels: $I_0=10$, 1, and 0.1. The initial dark band bending V_{so} was 0.6 V.

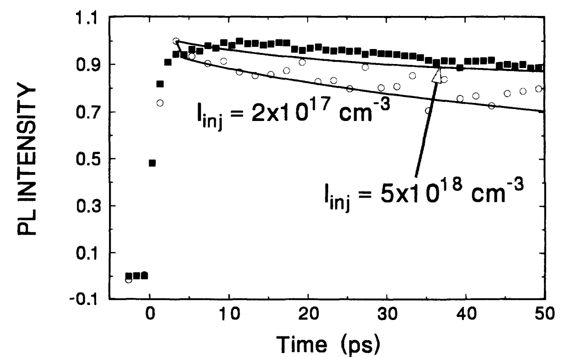

FIG. 10. Experimental and calculated (solid lines) PL decay curves for *p*-InP in air under high and moderate injection conditions. The solid lines were calculated with the same parameters (given in the text) except for the initial injection levels I_0.

and S_{pf} (the front SRV for electrons and holes, respectively) required for the best fit of the data were both 9×10^3 cm/s. All the carrier transfer velocities (S_{nft}, S_{pft}, S_{nbt}, and S_{pbt}) were zero, because the experiment was performed under open-circuit conditions.

The very fast initial PL decay ($t<5$ ps) observed in the lower curve is due to the electron-hole separation in the SCR, as discussed in previous sections; this SCR region is formed due to intrinsic surface states at the *p*-InP air interface. When $I_0=30$ (the upper curve) the SCR field is instantaneously screened by the photogenerated carriers, and the PL intensity starts to decrease only after about 10 ps. This PL rise time is due to carrier cooling effects; under these high-injection levels it takes on the order of 10 ps for the hot electrons created by the excitation pulse to reach the bottom of the conduction band.[22,23] Our model currently does not include these effects. The rise time observed for the lower curve is only around 3–4 ps due to the faster electron cooling rate at the lower injection levels.

B. Time-correlated single-photon counting—picosecond time resolution

The structure used for these measurements was a heterostructure device consisting of 0.5-μm-thick *p*-GaAs (Zn doped, 5×10^{16} cm^{-3}) grown on a heavily Zn-doped GaAs substrate, and capped with a 40-Å-thick layer of $Ga_{0.52}In_{0.48}P$. All the structures were grown in a vertical, atmospheric-pressure organometallic chemical vapor (OMCVD) deposition reactor described in detail elsewhere.[24] Pieces cleaved from the samples were mounted in a photoelectrochemical (PEC) electrode configuration according to procedures described previously.[25] The redox couple was 0.5-M cobaltocenium $[Co(Cp)_2{}^+]$ plus 0.05-M cobaltocene; bias voltages quoted here are versus a Pt reference electrode.

The TRPL measurements were carried out using a synch-pumped cavity-dumped dye laser operating at a wavelength of 600 nm, at a repetition rate of 800 Khz, and with a pulse width of 5 ps. The luminescence was collected using a time-correlated single-photon-counting apparatus with a system response time of 35 ps.

As mentioned above, these experiments were carried out under ideal conditions: i.e., very low SRV, and under the effect of well-defined and controlled electric fields. The $Ga_xIn_{1-x}P$-capped GaAs was found to be an ideal system for these purposes: the 40-Å barrier gave very low interface recombination velocities,[26] and was very stable in contact with the solution. The external bias was controlled by a potentiostat, and the surface band bendings at each applied voltage were determined from Mott-Schottky (MS) plots using standard procedures.[25]

Figure 11 shows the MS plot of the above structure measured under pulsed laser illumination. The arrows show the four potentials and band-bending values at which the TRPL spectra (shown in Fig. 12) were recorded. This plot was used for obtaining the band-bending values under the laser excitation conditions; these values are shown as labels for the arrows in Fig. 11. The band-banding values were justified based on the following arguments. First, the excess carriers generated by the picosecond laser pulse have a lifetime of about a couple of ns; this is, of course, not detected by the lock-in amplifier used for the MS measurements. Hence the extracted band bending is to an excellent approximation not affected by the pulsed nature of the laser. Second, band movement effects (due to surface state charging) are only affected by the magnitude of the average laser power. This was verified by measuring the MS plots under different laser repetition rates; the results were identical in the range of 40 Khz to 80 Mhz. In summary, the band-bending values obtained from the laser-illuminated MS plots shown in Fig. 11 were used as the V_{so} values in the TRPL calculations.

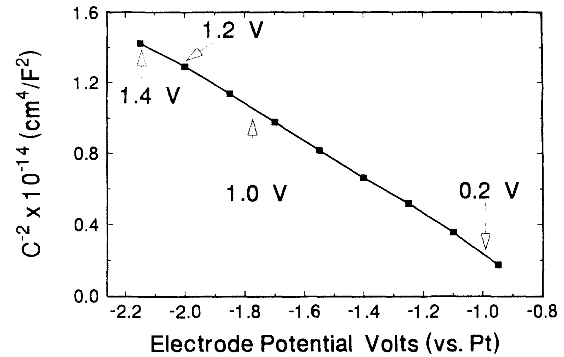

FIG. 11. Mott-Schottky plot for the 40-Å $Ga_xIn_{1-x}P$/*p*-GaAs heterostructure in 0.5-M $CoCp_2^+$ measured under the pulsed laser illumination, and at a frequency of 20 kHz. The arrows show the four potentials and band-bending values at which the TRPL spectra (shown in Fig. 12) were recorded.

Figure 12 shows the TRPL decay curves of the $GaAs/Ga_xIn_{1-x}P$ heterostructure measured at four different potentials which correspond to actual band bendings of 0.0–0.6, 1.0, 1.2, and 1.4 V, as shown in Fig. 11; this was based on a flat-band potential of 0.8 V (vs the Pt electrode). The solid lines in Fig. 12 were calculated using the following known parameters: $\alpha=4\times10^4$ cm^{-1}, $\alpha_L=2\times10^3$ cm^{-1}, $\mu_n=3800$ cm^{2}V^{-1}s^{-1}, $\mu_p=190$

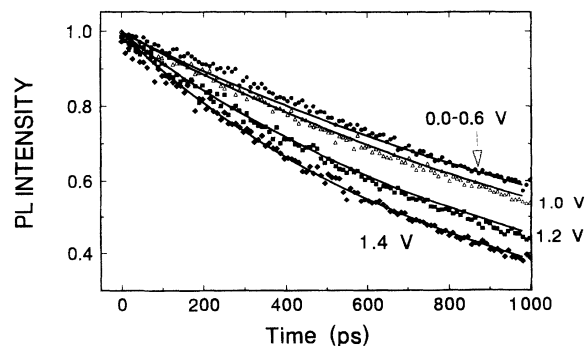

FIG. 12. Experimental and calculated (solid lines) PL decay curves for the 40-Å $Ga_xIn_{1-x}P$/*p*-GaAs heterostructure in 0.5-M $CoCp_2^+$. The solid lines were calculated with the same parameters (given in the text) except for the initial band-bending values shown in the figure.

$cm^2 V^{-1} s^{-1}$, and $B = 2\times10^{-10}$ $cm^3 s^{-1}$; selection of the values of the above fixed parameters were based on previous studies of GaAs.[4] The values of the bulk nonradiative lifetime and the recombination velocities at the two interfaces were obtained by measuring the TRPL of identical heterojunctions with different epilayer thicknesses;[24] this yielded the following values: $S_{nf} = S_{pf} = 250$ cm/s, $S_{nb} = S_{pb} = 900$ cm/s, and $\tau_n = \tau_p$ 12 ns. All the calculated carrier transfer velocities (S_{nft}, S_{nbt}, S_{pft}, and S_{pbt}) were found to be much lower than the above SRV's. This result was supported by photocurrent quantum yield measurements that gave yields below 10%;[21] this was attributed to slow tunneling (relative to the recombination rate) through the 40-Å barrier. A $\delta(t)$ laser pulse was assumed, and the initial injection level I_0 was 0.5 based on the measured laser spot size and incident laser power.

The calculated decay curves in Fig. 12 show quite a good agreement with the experimental data. In the potential range of 0.0–0.6 V there is a very small effect on the PL decay rate; only when the band bending is increased to 1.0 V is there a notable change in the TRPL spectra. This could be explained in the following way. As mentioned earlier, an increase in the band-bending magnitude causes the effective recombination velocity to increase. In a thin epilayer, the PL decay time τ_{PL} can be approximated by[24]

$$\tau_{PL}^{-1} = \tau_B^{-1} + \frac{(S_{eff}^b + S_{eff}^f)}{d} , \qquad (12)$$

where τ_B is the bulk effective lifetime, and S_{eff}^b and S_{eff}^f are the effective recombination velocities of the back and front interfaces, respectively. With increasing reverse bias S_{eff}^f will increase, and it will reduce τ_{PL} only when $(S_{eff}^b + S_{eff}^f)/d > 1/\tau_B$; this requires that S_{eff}^f will be greater than ~4000 cm/s. In the present case this happens only at band bending greater than 0.6 V. This is in agreement with the dependence of S_{eff} on band bending and injection levels, as was calculated recently by us.[27]

The results in Fig. 12 show that when the SRV at zero field is very low, as in the $GaAs/Ga_xIn_{1-x}P$ interface measured here, the effective SRV has increased to relatively small values even in the presence of very large electric fields. In TRPL spectra and device analysis it is usually assumed that S_{eff} is very high ($>1\times10^7$ cm/s) when a SCR is present. In a recent paper[28] we have shown that the necessary conditions for such large S_{eff} are (1) the field free SRV is $>1\times10^4$ cm/s; (2) $V_{so} > 0.5$ V; and (3) the initial injection level I_0 is <0.1. This implies that assigning very high S_{eff} in device analysis is *not* always a good approximation.

The PL decay rate can also increase due to field-enhanced charge transfer to the adjacent solution through the $Ga_xIn_{1-x}P$ barrier. This tunneling process was suppressed here by the 40-Å $Ga_xIn_{1-x}P$ barrier. In experiments carried on heterojunctions with 20-Å-thick barriers, a large increase in the PL decay rate with increasing negative bias was observed; this was attributed to field-enhanced tunneling through the thinner barrier.

The low-carrier transfer velocities obtained from the data in Fig. 12 are in contrast to the ultrahigh values we have observed with other electrodes and redox acceptors when the initial band bending increases above about 0.5 V. Thus, for example, with *p*-InP electrodes and $Fe(CN)_6^{3-}$ acceptors in aqueous electrolyte, S_{nft} was found to rise to 5×10^7 cm/s when the initial band bending was >0.5 eV.[28] These differences are attributed to the vastly different rate constants for electron transfer that depend on the nature of the acceptor and photoelectrode. Our model enables us to determine these rate constants for different systems as a function of the applied electrode potential.

V. SUMMARY AND CONCLUSIONS

We have presented a rigorous analysis of the effect of electric fields on time-resolved luminescence spectra in semiconductors. The analysis, based on the drift-diffusion approximation for the semiconductor transport equations, shows that electric fields have a rich effect on the TRPL spectra.

Under high initial injection conditions the SCR electric field is screened by the photogenerated carriers in less than 0.2 ps, and hence the TRPL spectra are not affected by the applied bias. At a lower injection level (when the initial excess carrier concentration is equal to the doping level) the TRPL spectra are affected by the electric field. The PL is quenched in the first few picoseconds due to the electron-hole spatial separation; with increasing applied bias the depletion region width increases, and the effect on the TRPL spectra is larger. Under low-injection levels the shape of the PL decay is quite different. This is caused by the fact that the surface bend bending is reduced only by about a factor of 0.6–0.7 times its original dark value; therefore the luminescence decay is governed by a large S_{eff}, which increases the PL decay rate.

We have found good agreement with the calculations and two different sets of experiments. In the first we showed that under an intermediate injection level the charge separation in the SCR affects the PL decay in the first few picoseconds, as predicted by the model. Under very-high-injection conditions the SCR field is screened, in agreement with the calculations.

The second group of experiments showed the effect of the electric fields on the luminescence decay under a low-injection level and closed-circuit conditions. It was found that when the SRV at zero field is very low, as in the $GaAs/Ga_xIn_{1-x}P$ interface measured here, the effective SRV has increased to relatively small values even in the presence of very large electric fields. This result emphasizes one of the important contributions of our model. It enables the extraction of the recombination or transfer velocity when a SCR is present.

ACKNOWLEDGMENTS

This work was supported by the U.S. Department of Energy, Office of Energy Research, Division of Basic Energy Sciences, Chemical Sciences Division. We thank C. L. Tang and R. J. Ellingson for collaboration in the upconversion experiments, and J. M. Olson and K. Bertness for supplying the $Ga_xIn_{1-x}P/GaAs$ samples.

[1]T. Held, T. Kuhn, and G. Mahler, Phys. Rev. B **44**, 12 873 (1991), and references within.

[2]X. Zhou, T. Hsiang, and R. J. D. Miller, J. Appl. Phys. **66**, 3066 (1989); T. Dekorsy, T. Pfeifer, W. Kutt, and H. Kurz, Phys. Rev. B **47**, 3842 (1993).

[3]J. A. Kash, E. E. Mendez, and H. Morkoc, Appl. Phys. Lett. **46**, 173 (1985).

[4]Y. Rosenwaks, B. R. Thacker, R. K. Ahrenkiel, and A. J. Nozik, J. Phys. Chem. **96**, 10 097 (1992); L. A. Gomez-Jahn and R. J. D. Miller, *ibid.* **96**, 3981 (1992).

[5]A. J. Nozik, F. Williams, and D. Boudreaux, J. Appl. Phys. **51**, 2158 (1980).

[6]A. J. Nozik and R. T. Ross, J. Appl. Phys. **53**, 3813 (1982).

[7]A. J. Nozik and F. Williams, Nature **311**, 21 (1984).

[8]J. Shah, IEEE J. Quantum Electron. **QE-24**, 276 (1988); D. W. Bailey and C. J. Stanton, Appl. Phys. Lett. **60**, 880 (1992).

[9]R. K. Ahrenkiel, in *Semiconductors and Semimetals,* edited by R. K. Ahrenkiel and M. S. Lundstrom (Academic, London, 1993), Vol. 39, pp. 39–150, and references within.

[10]Y. Rosenwaks, Y. Shapira, and D. Huppert, Appl. Phys. Lett. **57**, 2552 (1990).

[11]G. W. 't Hooft and C. van Opdrop, J. Appl. Phys. **60**, 1065 (1986).

[12]D. Edelstein, C. L. Tang, and A. J. Nozik, Appl. Phys. Lett. **51**, 48 (1987).

[13]The effects of the electric field are most commonly minimized by conducting the experiments under flat-band conditions; see, for example, Y. Rosenwaks, Y. Shapira, and D. Huppert, Phys. Rev. B **45**, 9108 (1992).

[14]Lateral carrier transport can be neglected when defocused laser excitation is used.

[15]M. L. Shumaker, W. J. Dollard, and D. H. Waldeck, J. Phys. Chem. **96**, 10 371 (1992).

[16]J. F. Kauffman, B. A. Balko, and G. L. Richmond, J. Appl. Phys. **73**, 1912 (1993).

[17]A. Ehrhardt, W. Wettling, and A. Bett, Appl. Phys. A **53**, 123 (1991).

[18]S. R. Dhariwal and D. R. Mehrotra, Solid State Electron. **88**, 1355 (1988), and references within.

[19]Such time resolution in luminescence detection (usually achieved by up-conversion) requires an initial carrier concentration above 5×10^{16} cm^{-3}; see, for example, F. Wise and C. L. Tang, Solid State Commun. **69**, 821 (1989).

[20]S. Selberherr, *Analysis and Simulation of Semiconductor Devices* (Springer-Verlag, New York, 1984), p. 20.

[21]D. G. McLean, M. G. Roe, A. I. D'Souzg, and P. E. Wigen, Appl. Phys. Lett. **48**, 992 (1986).

[22]Y. Rosenwaks, M. C. Hanna, D. H. Levi, D. M. Szmyd, R. K. Ahrenkiel, and A. J. Nozik, Phys. Rev. B **97**, 10 421 (1993).

[23]W. S. Pelouch, R. J. Ellingson, P. E. Powers, C. L. Tang, D. Szmyd, and A. J. Nozik, Phys. Rev. B **45**, 1450 (1992).

[24]J. M. Olson, R. K. Ahrenkiel, O. J. Dunlavy, B. Keyes, and A. E. Kibbler, Appl. Phys. Lett. **55**, 1208 (1989).

[25]G. Cooper, J. A. Turner, B. A. Parkinson, and A. J. Nozik, J. Appl. Phys. **54**, 6463 (1983).

[26]Y. Rosenwaks and A. J. Nozik (unpublished).

[27]Y. Rosenwaks, A. J. Nozik, and I. Yavneh, J. Appl. Phys. **75**, 4255 (1994).

[28]Y. Rosenwaks, B. R. Thacker, A. J. Nozik, R. J. Ellingson, K. C. Burr, and C. L. Tang, J. Phys. Chem. **98**, 2739 (1994).

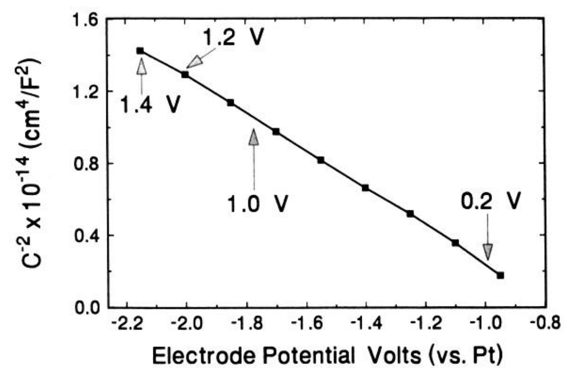

FIG. 11. Mott-Schottky plot for the 40-Å $Ga_xIn_{1-x}P/p$-GaAs heterostructure in 0.5-M $CoCp_2^+$ measured under the pulsed laser illumination, and at a frequency of 20 kHz. The arrows show the four potentials and band-bending values at which the TRPL spectra (shown in Fig. 12) were recorded.

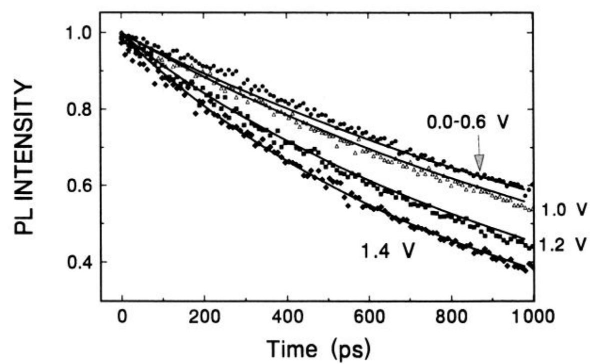

FIG. 12. Experimental and calculated (solid lines) PL decay curves for the 40-Å $Ga_xIn_{1-x}P/p$-GaAs heterostructure in 0.5-M $CoCp_2^+$. The solid lines were calculated with the same parameters (given in the text) except for the initial band-bending values shown in the figure.

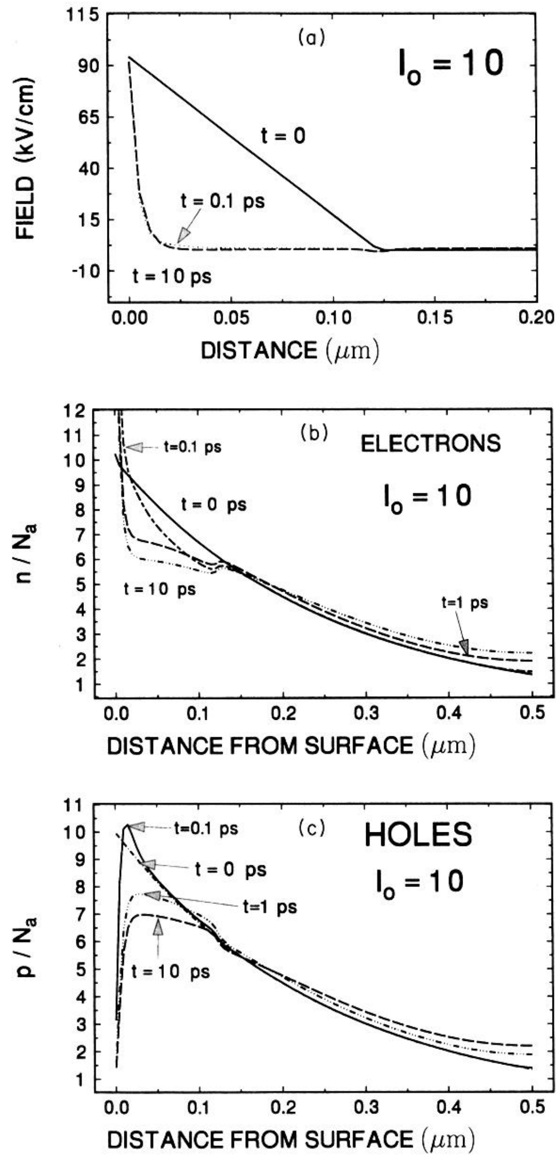

FIG. 4. (a) Electric-field profiles calculated before the laser pulse ($t=0$), and at $t=0.1$ (dotted line) and 10 ps after the excitation. The initial dark band bending V_{so} was 0.6 V. (b) Excess electrons distributions (normalized to the majority-carrier concentration N_a) at four different times after the excitation: $t=0$, 0.1, 1, and 10 ps. (c) Excess hole distributions at the same times as in (b).

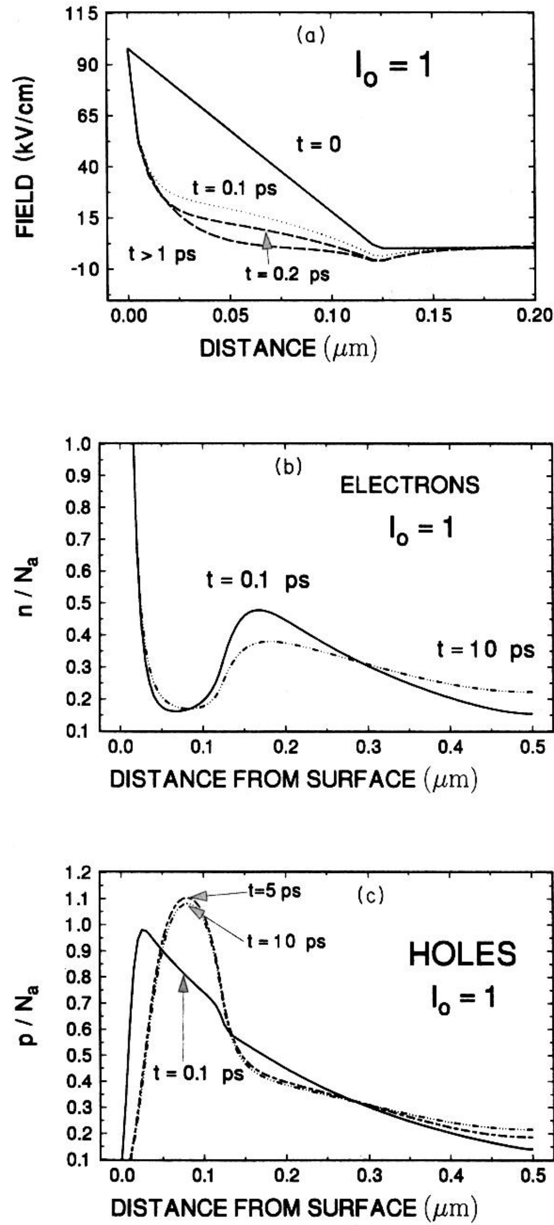

FIG. 6. (a) Electric-field profiles calculated at four different times relative to the laser pulse (at $t=0$). The initial dark band bending V_{so} was 0.6 V. (b) Excess electrons distributions (normalized to the majority-carrier concentration N_a) at two different times after the excitation: $t=0.1$ and 10 ps. (c) Excess hole distributions at times of 0.1, 5, and 10 ps following the excitation.